[^{18}F]MK-9470, a positron emission tomography (PET) tracer for *in vivo* human PET brain imaging of the cannabinoid-1 receptor

H. Donald Burns*†, Koen Van Laere‡, Sandra Sanabria-Bohórquez*, Terence G. Hamill*, Guy Bormans§, Wai-si Eng*, Ray Gibson*, Christine Ryan*, Brett Connolly*, Shil Patel*, Stephen Krause*, Amy Vanko*, Anne Van Hecken¶, Patrick Dupont‡, Inge De Lepeleire‖, Paul Rothenberg**, S. Aubrey Stoch**, Josee Cote**, William K. Hagmann††, James P. Jewell††, Linus S. Lin††, Ping Liu††, Mark T. Goulet††, Keith Gottesdiener**, John A. Wagner**, Jan de Hoon¶, Luc Mortelmans‡, Tung M. Fong‡‡, and Richard J. Hargreaves*

*Imaging Research, Merck Research Laboratories, West Point, PA 19486; ‡Division of Nuclear Medicine, University Hospital and Katholieke Universiteit Leuven, B-3000 Leuven, Belgium; §Laboratory for Radiopharmacy and ¶Centre for Clinical Pharmacology, Katholieke Universiteit Leuven, B-3000 Leuven, Belgium; ‖Merck Research Laboratories, B-1180 Brussels, Belgium; ‡‡Metabolic Disorders and ††Medicinal Chemistry, Merck Research Laboratories, Rahway, NJ 07065; and **Clinical Pharmacology, Merck Research Laboratories, Upper Gwynedd, PA 19454

Communicated by Michael E. Phelps, University of California School of Medicine, Los Angeles, CA, April 20, 2007 (received for review November 15, 2006)

[^{18}F]MK-9470 is a selective, high-affinity, inverse agonist (human IC_{50}, 0.7 nM) for the cannabinoid CB1 receptor (CB1R) that has been developed for use in human brain imaging. Autoradiographic studies in rhesus monkey brain showed that [^{18}F]MK-9470 binding is aligned with the reported distribution of CB1 receptors with high specific binding in the cerebral cortex, cerebellum, caudate/putamen, globus pallidus, substantia nigra, and hippocampus. Positron emission tomography (PET) imaging studies in rhesus monkeys showed high brain uptake and a distribution pattern generally consistent with that seen in the autoradiographic studies. Uptake was blocked by pretreatment with a potent CB1 inverse agonist, MK-0364. The ratio of total to nonspecific binding in putamen was 4–5:1, indicative of a strong specific signal that was confirmed to be reversible via displacement studies with MK-0364. Baseline PET imaging studies in human research subject demonstrated behavior of [^{18}F]MK-9470 very similar to that seen in monkeys, with very good test–retest variability (7%). Proof of concept studies in healthy young male human subjects showed that MK-0364, given orally, produced a dose-related reduction in [^{18}F]MK-9470 binding reflecting CB1R receptor occupancy by the drug. Thus, [^{18}F]MK-9470 has the potential to be a valuable, noninvasive research tool for the *in vivo* study of CB1R biology and pharmacology in a variety of neuropsychiatric disorders in humans. In addition, it allows demonstration of target engagement and noninvasive dose-occupancy studies to aid in dose selection for clinical trials of CB1R inverse agonists.

inverse agonist occupancy

Marijuana (*Cannabis sativa*) has been of interest for its psychotropic and potential therapeutic effects for thousands of years and recently has received substantial attention from the pharmaceutical industry as a potential source of novel treatments for a wide variety of neuropsychiatric conditions including multiple sclerosis (1), pain and nausea (2–4), glaucoma (5), levodopa-induced dyskinesia in Parkinson's disease (6–10). The actions of this herb are thought to stem mainly from the agonist interaction of its major active component, Δ^9-tetrahydrocannabinol (Δ^9-THC), with either of two known cannabinoid receptor subtypes: cannabinoid-1 receptor (CB1R), found mainly in the brain (11), and CB2R, found mainly in immune system cells in the periphery and in only minute amounts in the normal CNS (12). By using autoradiographic and immunohistochemical techniques in postmortem human brain, it has been found that CB1R are distributed with high density in substantia nigra, globus pallidus, putamen, hippocampus, and cerebellum (13, 14).

Of particular recent interest is the role that CB1R and its endogenous ligands play in feeding behavior (15) and in addiction (16, 17). It is well known that Δ^9-THC stimulates food intake (18) and CB1R knockout mice are lean and resistant to diet-induced obesity (19). Rimonabant (SR-141716A), a CB1R inverse agonist, was recently approved in the 25 states of the European Union for the treatment of obesity (*Management Report for the First Half of 2006* from Sanofi Aventis; available at http://en.sanofi-aventis.com/Images/060630_halfreport2006_en_tcm24-13284.pdf).

Over the past decade, substantial effort has been invested in developing CB1R single-photon emission computed tomography and positron emission tomography (PET) ligands to allow *in vivo* imaging of this receptor system. Such ligands would be valuable tools for the investigation of CB1R neurobiology. Endogenous CB1R ligands have only moderate affinity and are highly lipophilic, thus not likely to be satisfactory as *in vivo* single-photon emission computed tomography or PET ligands. Successful *in vivo* ligands are generally high affinity and only moderately lipophilic. High nonspecific binding and low brain penetration are normally seen with lipophilic compounds. Most reported efforts at developing ligands for *in vivo* imaging of CB1R have focused on single-photon emission computed tomography or PET radiotracers based on the 1,5-diaryl-3-carboxypyrazole structure of SR-141716A that are also highly lipophilic.

Of these, [^{123}I]AM251 [supporting information (SI) Table 2] failed to show significant brain uptake in the baboon brain (20). The less lipophilic [^{123}I]AM281 was more promising as an imaging agent, showing higher brain uptake, especially in the CB1R-rich cerebellum that was partially blocked by pretreatment with SR-141716A (21). More recently, [^{123}I]AM281 has been used in clinical studies of Δ^9-THC therapy of Tourette patients (22) to determine

Author contributions: H.D.B., K.V.L., S.S.-B., T.G.H., W.-s.E., R.G., C.R., P.R., S.A.S., J.C., W.K.H., J.P.J., L.S.L., P.L., M.T.G., K.G., J.A.W., T.M.F., and R.J.H. designed research; K.V.L., S.S.-B., T.G.H., G.B., W.-s.E., R.G., C.R., B.C., S.P., S.K., A.V., A.V.H., P.D., I.D.L., W.K.H., J.P.J., L.S.L., P.L., M.T.G., J.d.H., and L.M. performed research; T.G.H. and G.B. contributed new reagents/analytic tools; H.D.B., S.S.-B., G.B., W.-s.E., R.G., B.C., S.P., A.V., P.R., S.A.S., J.C., K.G., T.M.F., and R.J.H. analyzed data; and H.D.B., K.V.L., S.S.-B., T.G.H., G.B., W.-s.E., R.G., C.R., B.C., A.V.H., P.D., I.D.L., S.A.S., K.G., J.A.W., J.d.H., L.M., T.M.F., and R.J.H. wrote the paper.

The authors declare no conflict of interest.

Freely available online through the PNAS open access option.

Abbreviations: Δ^9-THC, Δ^9-tetrahydrocannabinol; CB1R, cannabinoid-1 receptor; PET, positron emission tomography; AUC, area under the curve; TAC, time–activity curve; SUV, standardized uptake value.

†To whom correspondence should be addressed at: Nuclear Imaging Research, Merck Research Laboratories, WP44D-225, Sumneytown Pike, West Point, PA 19486. E-mail: donald_burns@merck.com.

This article contains supporting information online at www.pnas.org/cgi/content/full/0703472104/DC1.

www.pnas.org/cgi/doi/10.1073/pnas.0703472104

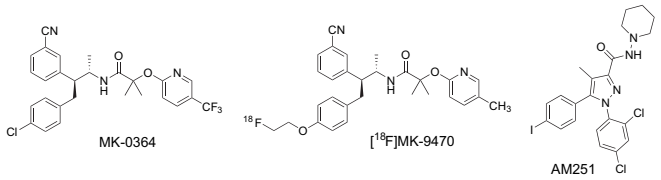

Fig. 1. Chemical structure of CB1R-selective PET tracer, [^{18}F]MK-9470; MK-0364, a structurally analogous CB1R inverse agonist used in the occupancy drug studies in this paper; and AM251, a structurally unique CB1R inverse agonist used as the blocking compound in the autoradiographic studies.

whether [^{123}I]AM281 distribution matches the known distribution of CB1R and whether decreased tracer binding could be detected during Δ^9-THC therapy. [^{123}I]AM281 demonstrated a low specific signal, and 3-week Δ^9-THC treatment had no significant effect on specific signal in a group of four patients. A study using [^{124}I]AM281 in one schizophrenic patient showed low brain uptake and very poor contrast (23).

Recently, several groups have developed novel ^{11}C-labeled PET tracers[§§] with promising characteristics (see SI Table 2 for structures). [^{11}C]JHU75528, a tracer with good binding affinity and relatively low nonspecific binding, was reported recently (24). In baboon brain imaging studies, the expected distribution of the tracer was observed with the binding potential in the putamen of 1.3–1.5. Tracer uptake was blocked with unlabeled JHU75528 or rimonabant. [^{11}C]SD 5024 (25) also shows appropriate characteristics of brain penetration and specific binding and is in further investigation.,

As part of our CB1R inverse agonist drug development program, we developed [^{18}F]MK-9470 (see Fig. 1 and Table 1), an ^{18}F-labeled, selective, high-affinity inverse agonist CB1R PET radiotracer. We have shown in preclinical and clinical imaging studies that this tracer is a useful tool for noninvasive studies of CB1R biology/pharmacology and for use in measuring receptor occupancy of potential therapeutic CB1R inverse agonists. We report here the radiosynthesis, preclinical characterization, and results of PET imaging studies in rhesus monkeys and healthy human volunteers of [^{18}F]MK-9470.

Results

Receptor Affinity and Specificity. MK-9470 (Fig. 1) is a potent CB1R inverse agonist with 0.7 nM binding affinity for the human CB1R and a 60-fold selectivity for CB1R over CB2R (Table 1). Extensive *in vitro* screening against >100 cerebral receptors/ion channels revealed no significant off-target activities. A total of six targets had affinities <5 μM, with the affinities ranging from 0.5 to 2.7 μM.

Autoradiography Distribution. [^{18}F]MK-9470 was evaluated in *ex vivo* binding studies by using rhesus brain sections. As shown in Fig. 2, the anatomical distribution of binding sites is consistent with the reported localization of CB1R in the brain of various mammalian species and supports the specificity of [^{18}F]MK-9470 for this site. Cerebral cortex, cerebellum, caudate/putamen, globus pallidus, substantia nigra, and hippocampus were areas of intense positive signal. Posterior hypothalamus, ventral tegmental area, and periventricular gray area all showed moderate signals, and the lowest signal was found in the thalamic nuclei. Addition of the inverse agonist AM251 effectively blocked specific binding.

***In Vivo* Rhesus Monkey Imaging.** Baseline PET scans showed rapid brain penetration and accumulation of [^{18}F]MK-9470 in most gray matter regions of the brain as expected for binding to CB1R and consistent with autoradiography results. Uptake in white matter was significantly lower. Results of scans acquired after i.v. bolus plus constant infusion of MK-0364 (Fig. 1) to steady-state plasma levels of ≈1 μM showed substantial reduction in [^{18}F]MK-9470 binding in gray matter to a level very close to that in white matter. The specific signal observed was ≈5:1 (total/nonspecific) in one monkey and ≈4:1 in another (Fig. 3) for several key regions of the brain (cerebellum, frontal cortex, putamen, and thalamus). Other gray matter regions behaved similarly.

To determine whether the observed binding is reversible, a rhesus imaging study was conducted with an i.v. bolus administration of MK-0364 (Fig. 3) given 120 min into a baseline scan with [^{18}F]MK-9470. This caused rapid washout of radioactivity from all gray matter regions in the brain, confirming reversibility of tracer binding to CB1 receptors.

Table 1. Human CB1R binding IC_{50} values and functional EC_{50} values of MK-9470

Receptor	IC_{50}, nM (*n*)	EC_{50}, nM	% activity relative to CP55940
CB1R	0.7 (4)	0.9	−127
CB2R	44 (4)	8	−225

Rhesus Occupancy Studies. Taken together, these previous results demonstrate that [^{18}F]MK-9470 is a very well behaved, CB1R-selective tracer in the rhesus monkey. We therefore used it to establish occupancy/dose and occupancy/plasma level relationships for MK-0364 in a group of three rhesus monkeys (SI Table 3).

Occupancy for each postdose scan was calculated and plotted vs.

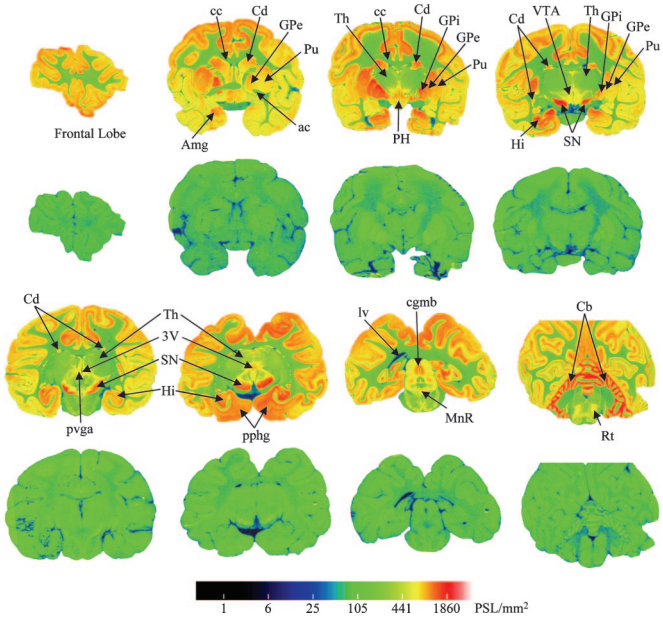

Fig. 2. Autoradiographic distribution of bound [^{18}F]MK-9470 in the rhesus brain. Coronal sections (20 μm) of rhesus brain were incubated with [^{18}F]MK-9470. Specific binding was assessed by incubating replicate sections with (lower two rows) and without (upper two rows) 1×10^{-5} M AM251, a structurally unique CB1R inverse agonist. The sections were exposed to phosphorimaging plates for 20 min, scanned, and analyzed with MCID software. Amg, amygdala; Cb, cerebellum; cc, corpus callosum; Cd, caudate; cgmb, central gray substance midbrain; Gpe, external globus pallidus; Gpi, internal globus pallidus; Hi, hippocampus; lv, lateral ventricle; MnR, median raphe nucleus; PH, posterior hypothalamus; pphg, posterior hippocampal gyrus; Pu, putamen; pvga, periventricular gray area; Rt, reticular nucleus; SN, substantia nigra; Th, thalamic nuclei; VTA, ventral tegmental area; 3V, third ventricle.

[§§]A report (50) on [^{11}C]MePPEP, another PET tracer for the CB1R, appears promising on the basis of preclinical studies.

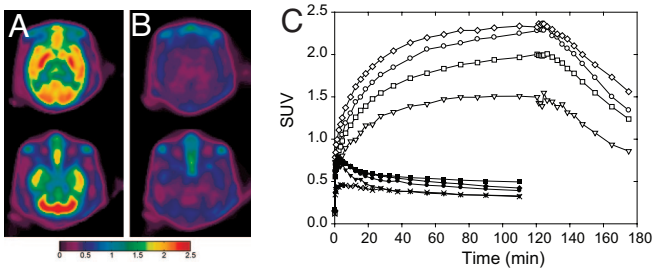

Fig. 3. *In vivo* PET images of [^{18}F]MK-9470 in rhesus monkey brain. (*A*) Baseline images (section through the basal ganglia and cerebellum, 60–120 min after tracer injection) demonstrate high tracer uptake in the brain with a regional distribution consistent with the known *in vitro* CB1R distribution. (*B*) [^{18}F]MK-9470 PET images acquired after MK-0364 dosing via bolus plus constant infusion to steady-state plasma levels sufficient to provide a high level of blockade of CB1R. Color scale indicates SUV units. (*C*) TACs with open symbols showing tracer binding in baseline conditions (0–120 min). At 120 min into the baseline scan, a chase MK-0364 dose was administered via bolus plus constant infusion, resulting in rapid displacement of the tracer from the CB1R, confirming reversible binding. ○, putamen; □, occipital cortex; ◇, cerebellum; ▽, thalamus; and ×, white matter. Data are corrected for the physical decay of ^{18}F.

the plasma level of MK-0364 during the image acquisition time (expressed as the average of plasma level measured just before and just after the image was acquired). Results showed good correlation between occupancy and steady-state plasma level, with very high blockade of tracer binding achieved at the highest levels tested, as shown in Fig. 4.

***In Vivo* Human Imaging.** [^{18}F]MK-9470 exhibited relatively slow brain kinetics reaching a plateau at ≈120 min after bolus injection (Fig. 5*B*). Tracer uptake was observed in all gray matter regions and remained relatively constant from 120 to 360 min after tracer injection. The greatest levels of uptake were observed in the striatum, frontal cortex, and posterior cingulate, whereas intermediate uptake was seen in the cerebellum and the lowest uptake was observed in the thalamus and hippocampus (Fig. 5*A*).

[^{18}F]MK-9470 metabolite analysis. The appearance of labeled metabolites in arterial plasma after [^{18}F]MK-9470 bolus injection is depicted in Fig. 5*C* for the four subjects in the test–retest panel. At 10 min, 77 ± 5% (n = 8) of the total radioactivity in arterial plasma corresponded to [^{18}F]MK-9470. This declined to 33 ± 5% at 60 min, 18 ± 3% at 120 min, and 13 ± 3% at 180 min. For the first two

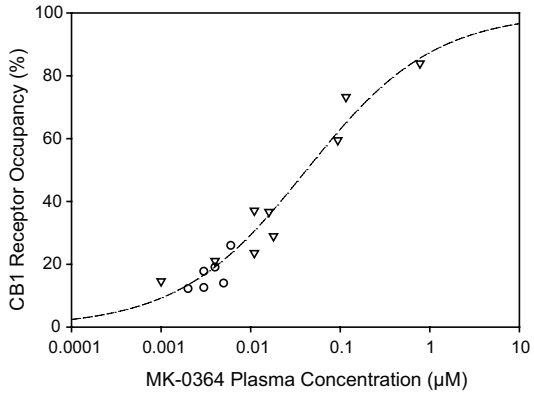

Fig. 4. Relationship between MK-0364 plasma concentration and *in vivo* CB1R occupancy measured by using [^{18}F]MK-9470 in rhesus monkey brain. PET studies were performed after a single dose (▽) and multiple doses (○) of MK-0364. When the data were fitted by using a Hill equation (dashed line, n_H = 1 = slope of the Hill plot), the projected plasma concentration producing 50% receptor occupancy (Occ_{50}) was estimated to be 34 nM.

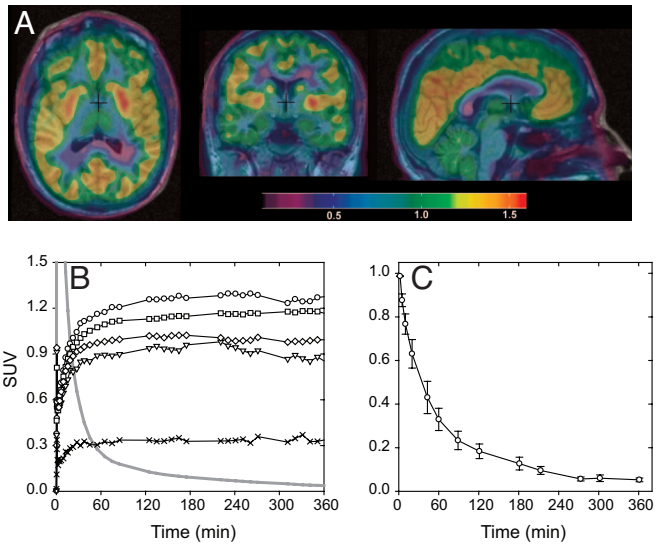

Fig. 5. Uptake of [^{18}F]MK-9470 in human brain. (*A*) Baseline images (120–180 min after tracer injection, day 1 of subject 1) show the regional distribution of tracer binding was consistent with labeling CB1R and with rhesus monkey images. Color scale corresponds to SUV units. (*B*) Tissue TACs (symbols) and [^{18}F]MK-9470 plasma curve (solid line). ○, putamen; □, occipital cortex; ◇, cerebellum; ▽, thalamus; and ×, white matter. Data are corrected for the physical decay of ^{18}F. (*C*) Average [^{18}F]MK-9470 fraction in arterial plasma (n = 8), as measured in the four subjects participating in the test–retest study. Error bars represent SD.

subjects, 6 ± 1% (n = 4) of the total radioactivity in arterial plasma corresponded to [^{18}F]MK-9470 at 270 min and 5 ± 1% (n = 4) at 360 min. Note that, although the input function decreases with time, the tissue activity remains relatively constant from 120 min to the end of the scan in all examined regions. These tracer kinetics in plasma and tissue suggest that [^{18}F]MK-9470 remains bound to CB1R for the duration of the scanning procedure, supporting the use of an area under the curve (AUC) analysis approach (49) for estimating receptor availability.

Test–retest studies. Reproducibility was evaluated in four subjects by scanning each subject twice, with an interval of ≈24 h between scans. Reproducibility was calculated by using the AUC of the second scanning segment, AUC(120–180 min), as 100 × abs[AUC(test) − AUC(retest)]/AUC(test). Within-subject test–retest variability was <7% for all regions for all four subjects. The between-subject variability in all regions for the four subjects in the test–retest study and the nine subjects (baseline condition) in the occupancy study described below was 16%.

Human CNS Occupancy by MK-0364. To illustrate feasibility of CNS CB1R occupancy determination by [^{18}F]MK-9470 in humans, we present the results of a CB1R occupancy study in nine healthy volunteers. Subjects received an oral dose of MK-0364 or placebo (n = 2) once a day for 14 days. The administered MK-0364 doses were as follows: 1.0 mg (n = 2), 4.0 mg (n = 3), or 7.5 mg (n = 2). Baseline scans were acquired before treatment, and posttreatment scans were performed ≈24 h after the last dose of MK-0364 or placebo. Imaging is illustrated in Fig. 6 for two subjects, one who was dosed with placebo and one who received 7.5 mg of MK-0364. Central CB1R occupancy data of this MK-0364 multiple-dose PET study are summarized in Fig. 7. For the two subjects receiving placebo, apparent CB1R occupancy was consistent with the test–retest estimates. The measured CB1R occupancies (±SD) after administration of 1.0, 4.0, and 7.5 mg of MK-0364 were 11 ± 1, 23 ± 7, and 41 ± 12%, respectively.

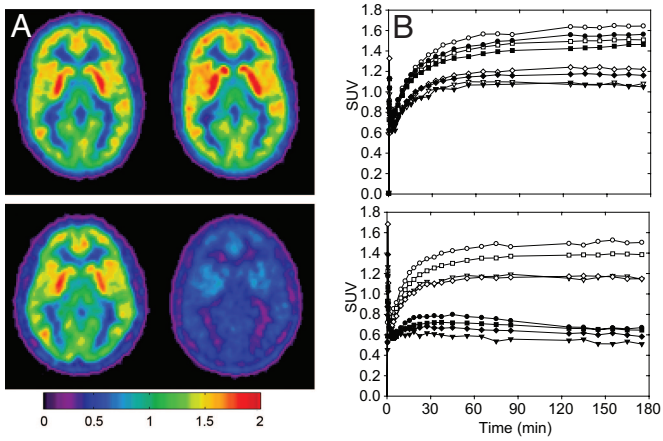

Fig. 6. PET images of CB1R were acquired in normal healthy male subjects before and after treatment with MK-3640 or placebo. (*A*) Representative transverse parametric SUV images at the level of the basal ganglia for two human subjects, acquired before (*Left*) and 24 h after (*Right*) treatment with either placebo (*Upper*) or a 7.5 mg dose of MK-0364 (*Lower*). (*B*) Graphs show the corresponding TACs: ○, putamen; □, occipital cortex; ◇, cerebellum; and ▽, thalamus. The open symbols denote baseline values, and the closed symbols denote the scan after treatment.

Discussion

The CB1R is one of the most abundant G protein-coupled receptors in the CNS, rivaling the abundance of benzodiazepine, striatal dopamine, and ionotropic glutamate receptors (14), and is 10-fold higher than that of opioid receptors (26). Expressed by all types of neural cells, including neurons, astrocytes, and oligodendrocytes (27), the postmortem regional distribution in the brain is heterogeneous and has been well characterized especially in rats (14, 26, 28–30) and also in humans (13, 31, 32). The findings of our monkey autoradiography data are in qualitative agreement with these studies, indicating suitability of the [^{18}F]MK-9470 for demonstrating CB1R sites in the brain *in vivo*.

In vitro, the observed affinity values for [^{18}F]MK-9470 (human IC_{50}, 0.7 nM) are slightly more potent than rimonabant, 2.2 nM (observed K_i value for [^{3}H]CP55940 displacement) (33). Moreover, affinity for the human CB1R is very high compared with the endocannabinoids AEA (anandamide) and 2-AG (2-arachidonoyl glycerol), which show affinities more toward the 26–209 μM range for AEA and even above 10 μM for 2-AG (34). These endocannabinoids also have poor selectivity for the CB1R over CB2R (35). Therefore, it is not clear whether endogenous action of the endocannabinoids is able to displace radiotracer binding, e.g., to study endocannabinoid release in analogy to dopamine (36).

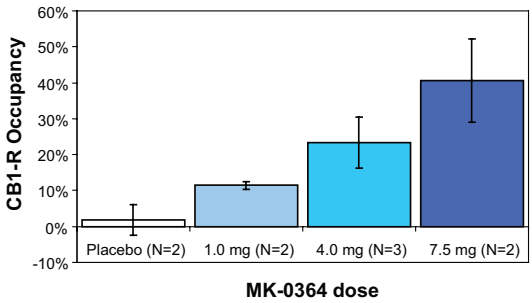

Fig. 7. Relationship between MK-0364 dose and CB1R occupancy using [^{18}F]MK-9470 in human brain. Baseline PET scans were performed before drug administration. Subjects received a daily dose of MK-0364 or placebo for 14 days and were scanned ≈24 h after the last dose. Error bars represent SD.

The development of radioligands for PET imaging of receptors in the CNS is a demanding task, and although binding has been demonstrated for many radioligands, only a few are suitable for applied quantitative studies (37). The human and rhesus monkey studies demonstrate that [^{18}F]MK-9470 can be used for quantitative CB1R occupancy assessment. Furthermore, the development of this radiotracer constitutes a major step into the characterization of the endocannabinoid system in human and animal CNS. *In vivo* occupancy determination allows for demonstration of target engagement and can aid in titration of dose regimen for subsequent clinical trials compared with pharmacokinetic profiling alone. Assessment of target engagement is critical in bridging from preclinical experiments to the clinic. Moreover, occupancy may also serve as a correlate of pharmacodynamic and safety parameters, as has been assessed extensively with the dopamine D_2 receptor system (38).

In humans, high CB1R receptor availability is found in frontal neocortical areas, subserving higher cognitive and executive functions, and in the posterior cingulate, a region pivotal for consciousness and higher cognitive processing (39). In humans, we observed ≈10% lower cerebellar CB1R binding compared with neocortical activity. This is at odds with the *in vivo* and *ex vivo* findings that highest CB1R expression in rats and monkeys is observed in the cerebellum. For humans, this is in line with the absence of gross motor disturbances after marijuana exposure and confirms recent immunohistochemical brain CB1R distribution data of membrane homogenates (40).

We have found relatively low *in vivo* [^{18}F]MK-9470 uptake in the hippocampus, pallidum, and substantia nigra. Especially for the latter two regions, partial volume effects due to the limited resolution of PET may have resulted in an underestimation of receptor availability. Neurochemical inhibition and enhanced green fluorescent protein microscopy studies, focused on the hippocampus, have suggested the presence of a large CB1R reserve of ≤85% located in intracellular vesicles (41–43). At present, it is unknown whether [^{18}F]MK-9470 binds to intracellular receptors. The observed differences between our *in vivo* CB1R expression study and reported postmortem research may be related to differences in the properties of the radioligand used. It is generally accepted that G protein-coupled receptor agonists have a higher affinity for the coupled receptor than for uncoupled receptor, whereas inverse agonists have a higher affinity for the uncoupled receptor than coupled receptor (44). The G protein level can also influence the ratio of coupled receptor to uncoupled receptor (45). Therefore, a radiolabeled agonist such as [^{3}H]CP55940 may report a quantitatively different CB1R density than that reported by a radiolabeled inverse agonist such as [^{18}F]MK-9470. Subtype selectivity does not account for the differences because only few CB2 receptors are present in the normal brain predominantly at the level of the brainstem (12).

Repeat studies were conducted in four subjects. Data analysis with the AUC method showed very good test–retest variability (≈7%), suggesting that this tracer will be a valuable tool for determination of CB1R occupancy and for studying regional CB1R receptor availability in the human brain under healthy conditions and in a variety of neuropsychiatric disorders. The between-subject variability in all regions was 16%, indicating higher physiological variability consistent with other known receptor systems such as dopamine or serotonin. The observed intersubject variability may be related to genetic polymorphisms in the CB1R (46), but also the use of standardized uptake value (SUV) as indicator for receptor availability may contribute. This variability needs to be investigated further with respect to aging, gender, and neuropsychological profile differences.

In conclusion, this study presents the successful *in vivo* characterization of CB1R distribution in healthy human brain by using PET imaging. *In vivo* PET imaging of CB1R provides a method for quantitative study of CB1R-related CNS pathophysiology and possible related therapeutic pathways involving the endocannabi-

noid system, which may play an important role in major neurological and psychiatric diseases such as neurodegeneration, eating disorders, substance abuse, schizophrenia, and depression. *In vivo* occupancy determination allows for demonstration of target engagement and assessment of titration for potential dose regimens.

Materials and Methods

Anesthetics. Ketamine (Ketaset) was obtained from Fort Dodge (Fort Dodge, IA), and propofol (Rapinovet) was obtained from Schering-Plough Animal Health (Union, NJ).

Chemical Synthesis of MK-9470 and Precursor to [^{18}F]MK-9470. MK-9470 (*N*-[2-(3-cyanophenyl)-3-(4-(2-[^{18}F]fluorethoxy)phenyl)-1-methylpropyl]-2-(5-methyl-2-pyridyloxy)-2-methylproponamide) (Fig. 1) and MK-9470-P, the phenol precursor to [^{18}F]MK-9470, were prepared in Merck's Good Manufacturing Practice Process Research facilities. Both MK-9470 and [^{18}F]MK-9470 were prepared from MK-9470-P by coupling with fluoroethylbromide (P.L., L.S.L., T.G.H., J.P.J., T. J. Lanza, Jr., R.G., S.K., C.R., W.-s.E., S.S.-B., *et al.*, unpublished work).

***In Vitro* and *in Vivo* Pharmacology.** *In vitro* binding studies were conducted as previously reported (47) with the exception that 4 mg/ml homogenate suspension was added to initiate the incubation.

Autoradiography. Autoradiographic studies were conducted as previously described (48) with rhesus monkey brain slices incubated for 2 h at room temperature in buffer containing either [^{18}F]MK-9470 alone or in combination with 10 μM AM251. Brain slices were then washed (three times for 3 min) with ice-cold buffer, rinsed with ice-cold distilled water, air dried, and placed on a tritium-sensitive phosphorimaging plate for 20 min, after which a Fuji (Tokyo, Japan) BAS5000 PhosphorImager was used to scan the phosphorimaging plates, regions of interest were drawn by using MCID Elite, and final images were prepared by using Photoshop.

Radiochemical Synthesis of [^{18}F]MK-9470 (Preclinical Studies). The description of the synthesis of [^{18}F]MK-9470 for preclinical and clinical studies can be found in the *SI Text*.

Rhesus Monkey Imaging Studies. Studies were conducted in four male rhesus monkeys (6–7 kg) under the guiding principles of the American Physiological Society and the *Guide for the Care and Use of Laboratory Animals* published by the National Institutes of Health and were approved by the West Point Institutional Animals Care and Use Committee at Merck Research Laboratories.

PET acquisitions were performed by using the ECAT EXACT HR+ (CTI/Siemens, Knoxville, TN) in 3D mode. Animals were anesthetized with ketamine (10 mg/kg, i.m.) followed by propofol (2 mg/kg, i.v. bolus plus a constant infusion of 0.4 mg·kg^{-1}·min^{-1}), intubated, and then ventilated by using medical grade compressed air at ≈100 ml per breath at a rate of 25 respirations per minute. Body temperature was maintained with circulating water heating pads, and temperature, SpO_2, and end-tidal CO_2 were monitored for the duration of the study. A bolus injection of ≈110 MBq of [^{18}F]MK-9470 was injected i.v. over 15 s with emission imaging initiating at the time of injection. For the chase study, the monkey was administered MK-0364 at 120 min after [^{18}F]MK-9470 injection. The chase dose consisted of a stock solution of 0.8 mg/ml MK-0364 (in a vehicle consisting of 15% EtOH, 40% PEG400, and 45% water) and was intravenously administered as a bolus (0.8 mg/kg) followed by constant infusion (0.64 mg·kg^{-1}·h^{-1}), and continued to the end of the scan (180-min total scan time).

Test–retest reproducibility was evaluated in all animals by performing at least two 90-min scans a week apart. Test–retest variability was <10%.

Approximately 1 week after the last baseline scan, conscious, fasted, chaired monkeys were administered a single oral dose (0.2, 1, 2, 3, 9, or 20 mg/kg) of MK-0364 via nasal gastric lavage as a solution in 15% ethanol/40% PEG400 in water. Follow-up scans were acquired at 5 h or 1, 3, or 7 days after dosing. In the multiple dosing studies, two monkeys received 0.5 mg daily doses of MK-0364 and underwent PET scans at 1, 5, and 8 days after dosing (SI Table 3). Plasma samples were collected during PET scans for determination of plasma levels of MK-0364.

Fig. 4 shows the resulting CB1R occupancy at the various doses used. The relationship between CB1R occupancy and MK-0364 plasma concentration (y) was described by using the Hill equation: Occupancy (%) = $A\ y^{n_H}/[(Occ_{50})^{n_H} + y^{n_H}]$. When the maximum occupancy A was set to 100% and the Hill coefficient n_H to 1, the projected plasma concentration producing 50% receptor occupancy (Occ_{50}) was estimated to be 34 nM.

Imaging Studies in Human Subjects. ***Subjects.*** All human imaging studies described here were conducted in the Division of Nuclear Medicine, University Hospital Leuven, Belgium. Thirteen healthy male volunteers (age range, 18–40 years) were recruited in response to advertisements in the University Hospital and community newspapers. Four subjects participated in a test–retest reproducibility substudy and the remaining nine subjects in the MK-0364 occupancy study. No control was placed on socioeconomic status or educational level. All underwent thorough physical examination, blood and urine testing (including toxicology for all major known addictive drugs), as well as high-resolution MRI T1 MPRAGE and routine T2 imaging. All investigations were performed by board-certified specialists.

Exclusion criteria based on history included known disorders of the CNS, head trauma with loss of consciousness, implanted electronic devices, substance abuse (alcohol, drugs, or psychoactive medication) or existing dependency or previous clinical treatment for complications of substance abuse, consumption of psychoactive medication during the past 3 months, or major internal disease. Urine testing included toxicology for benzodiazepines, neuroleptics, natural and synthetic opiates, cocaine and metabolites, amphetamines, and cannabinoids.

The study was approved by the local ethics committee and performed in accordance with the World Medical Association Declaration of Helsinki. Written informed consent was obtained from all of the volunteers before the study.

Imaging procedure. PET acquisitions were performed by using an HR+ camera (Siemens, Erlangen, Germany) in 3D mode. Subjects received on average 185 MBq of [^{18}F]MK-9470 in slow i.v. bolus injection. All subjects fasted for at least 4 h before measurements, and all measurements took place during daytime between 1100 and 1900 hours.

For the first two subjects (test–retest study), the scanning protocol consisted of four scanning segments separated by 30-min breaks with a total duration of 360 min. The first segment started simultaneously with the injection of the tracer and lasted 90 min. The remaining three segments had a total duration of 60 min (six 10-min frames) each and occurred at ≈120, 210, and 300 min. For these two subjects, CB1R index values estimated by using the 120–180 min interval differed from the corresponding values estimated by using the 120–360 min interval by ≤1%. Therefore, the scanning protocol for all other subjects consisted of the first two segments only (0–90 min and 120–180 min).

Blood sampling (test–retest study only). Before scanning, a radial artery cannula was inserted under local anesthesia for blood sampling. For total radioactivity assessment, 2-ml samples were withdrawn manually every 10 s for the first 2 min after tracer injection. Thereafter, the sampling interval increased progressively to ≈15 min. Three 2-ml blood samples were taken every 30 min during segments 2–4. Additional samples were taken for assessing the [^{18}F]MK-9470 unchanged fraction in plasma at 2, 5, 10, 20, 40, 60, and 90 min. For segments 2–4, 5-ml samples were taken at the beginning and end of the scanning period. For the two subjects

scanned for 180 min, only the samples at 10, 20, 40, 60 and 90, 120, and 180 min were taken for estimating [^{18}F]MK-9470 unchanged fraction.

[^{18}F]MK-9470 metabolite analysis. Acetonitrile (1 ml) was added to 1 ml of plasma and the mixture was centrifuged to precipitate protein. A 1-ml aliquot of the supernatant was filtered (Millex GV; Millipore, Bedford, MA; 0.22 μm, 13 mm in diameter) and injected onto the HPLC system [Waters, Milford, MA; C18 XTerra; 5 μm, 4.6 $\times$ 250 mm, 1.5 ml/min, 50:50 acetonitrile:50 mM sodium acetate (pH 5.5)]. HPLC eluants from 0–5 min (fraction 1, metabolite fraction) and 5–10 min (fraction 2, parent fraction) were collected. The amount of radioactivity in each fraction was counted in a γ counter to determine drug metabolism.

Image analysis. MRI and a [^{18}F]MK-9470 PET image obtained by summing all frames in the first acquisition segment were coregistered by using SPM99 (www.fil.ion.ucl.ac.uk/spm). Regions of interest were drawn in the basal ganglia, thalamus, cerebellum, frontal, parietal, occipital, medial, and lateral temporal cortex, hippocampus, and white matter (centrum semiovale) with the Montreal Neurological Institute DISPLAY software (www.bic.mni.mcgill.ca/software) by using the MRI for anatomical delineation. After alignment of all PET segments, tissue time–activity curves (TACs) were obtained by projecting the defined regions of interest onto all frames of the dynamic PET scans and expressed in SUV by using each subject's weight and the corresponding tracer injected dose as TAC (SUV) = TAC (becquerels) $\times$ 1,000 $\times$ subject's weight (kilograms)/injected dose (becquerels). Alignment between PET segments, TAC creation, and all subsequent analyses were performed by using in-house developed analysis software written in Matlab.

CB1R availability. The method of analysis used to estimate CB1R availability for occupancy determination was based on the TACs alone (49). The [^{18}F]MK-9470 plasma concentration became negligible during the study and [^{18}F]MK-9470 tissue concentration was essentially constant from 120 min to up to 6 h after tracer injection. Therefore, the area under the curve of the tissue TAC (AUC) after 120 min can be used as an index of CB1R availability.

Test–retest reproducibility. Each of the four subjects had two CB1R PET brain scans performed on consecutive days. No drug was administered to these subjects. The arterial line for input function estimation was kept in place overnight. Test–retest reproducibility was calculated by using AUC(120–180 min) as 100 $\times$ abs[1 $-$ AUC(day 2)/AUC(day 1)].

Receptor occupancy panels placebo vs. MK-0364 14-day multiple dose study. The study was double-blind, randomized, and placebo-controlled, with multiple panels designed to estimate brain CB1R occupancy of the inverse agonist MK-0364. Each subject underwent an initial [^{18}F]MK-9470 PET brain scan under baseline conditions. Then, subjects received a single, daily oral dose of MK-0364 or placebo for the next 14 days. Two subjects received placebo. The administered MK-0364 doses were as follows: 1.0 mg (n = 2), 4.0 mg (n = 3), or 7.5 mg (n = 2). Postdosing scans were conducted $\approx$24 h after the last dose of MK-0364. CB1R occupancy (CB1RO) after oral dosing with MK-0364 or placebo (PD) was calculated by using AUC(120–180 min) value under baseline (BL) conditions as 100 $\times$ [1 $-$ AUC(BL)/AUC(PD)].

K.V.L. was supported by a clinical research mandate of the Fund for Scientific Research (Flanders, Belgium). The human PET studies conducted at the Leuven University Hospital groups were supported by Merck.

1. Rog DJ, Nurmikko TJ, Friede T, Young CA (2005) *Neurology* 65:812–819.
2. Walker JM, Hohmann AG, Martin WJ, Strangman NM, Huang SM, Tsou K (1999) *Life Sci* 65:665–673.
3. Baker D, Pryce G, Croxford JL, Brown P, Pertwee RG, Huffman JW, Layward L (2000) *Nature* 404:84–87.
4. Berman JS, Symonds C, Birch R (2004) *Pain* 112:299–306.
5. Tomida I, Pertwee RG, Azuara-Blanco A (2004) *Br J Ophthalmol* 88:708–713.
6. Sieradzan KA, Fox SH, Hill M, Dick JP, Crossman AR, Brotchie JM (2001) *Neurology* 57:2108–2111.
7. Carroll CB, Bain PG, Teare L, Liu X, Joint C, Wroath C, Parkin SG, Fox P, Wright D, Hobart J, *et al.* (2004) *Neurology* 63:1245–1250.
8. van der Stelt M, Fox SH, Hill M, Crossman AR, Petrosino S, Di Marzo V, Brotchie JM (2005) *FASEB J* 19:1140–1142.
9. Hill MN, Gorzalka BB (2005) *Behav Pharmacol* 16:333–352.
10. D'Souza DC, bi-Saab WM, Madonick S, Forselius-Bielen K, Doersch A, Braley G, Gueorguieva R, Cooper TB, Krystal JH (2005) *Biol Psychiatry* 57:594–608.
11. Iversen L (2003) *Brain* 126:1252–1270.
12. Van Sickle MD, Duncan M, Kingsley PJ, Mouihate A, Urbani P, Mackie K, Stella N, Makriyannis A, Piomelli D, Davison JS, *et al.* (2005) *Science* 310:329–332.
13. Glass M, Dragunow M, Faull RL (1997) *Neuroscience* 77:299–318.
14. Herkenham M, Lynn AB, Little MD, Johnson MR, Melvin LS, De Costa BR, Rice KC (1990) *Proc Natl Acad Sci USA* 87:1932–1936.
15. Di Marzo V, Matias I (2005) *Nat Neurosci* 8:585–589.
16. Maldonado R, Valverde O, Berrendero F (2006) *Trends Neurosci* 29:225–232.
17. Lupica CR, Riegel AC (2005) *Neuropharmacology* 48:1105–1116.
18. Williams CM, Kirkham TC (2002) *Physiol Behav* 76:241–250.
19. Ravinet TC, Delgorge C, Menet C, Arnone M, Soubrie P (2004) *Int J Obes Relat Metab Disord* 28:640–648.
20. Gatley SJ, Gifford AN, Volkow ND, Lan R, Makriyannis A (1996) *Eur J Pharmacol* 307:331–338.
21. Gatley SJ, Lan R, Volkow ND, Pappas N, King P, Wong CT, Gifford AN, Pyatt B, Dewey SL, Makriyannis A (1998) *J Neurochem* 70:417–423.
22. Berding G, Muller-Vahl K, Schneider U, Gielow P, Fitschen J, Stuhrmann M, Harke H, Buchert R, Donnerstag F, Hofmann M, *et al.* (2004) *Biol Psychiatry* 55:904–915.
23. Berding G, Schneider U, Gielow P, Buchert R, Donnerstag F, Brandau W, Knapp WH, Emrich HM, Muller-Vahl K (2006) *Psychiatry Res* 147:249–256.
24. Horti AG, Fan H, Kuwabara H, Hilton J, Ravert HT, Holt DP, Alexander M, Kumar A, Rahmim A, Scheffel U, *et al.* (2006) *J Nucl Med* 47:1689–1696.
25. Donohue S, Halldin C, Finnema S, Gulyas B, Pike V (2006) *NeuroImage* 31:T50.
26. Herkenham M, Lynn AB, Johnson MR, Melvin LS, De Costa BR, Rice KC (1991) *J Neurosci* 11:563–583.
27. Ramirez BG, Blazquez C, Gomez del Pulgar T, Guzman M, De Ceballos ML (2005) *J Neurosci* 25:1904–1913.
28. Herkenham M, Lynn AB, De Costa BR, Richfield EK (1991) *Brain Res* 547:267–274.
29. Mailleux P, Vanderhaeghen JJ (1992) *Neurosci Lett* 148:173–176.
30. Tsou K, Brown S, Sanudo-Pena MC, Mackie K, Walker JM (1998) *Neuroscience* 83:393–411.
31. Mato S, Pazos A (2004) *Neuropharmacology* 46:716–726.
32. Westlake TM, Howlett AC, Bonner TI, Matsuda LA, Herkenham M (1994) *Neuroscience* 63:637–652.
33. Pertwee RG, Ross RA (2002) *Prostaglandins Leukot Essent Fatty Acids* 66:101–121.
34. Steffens M, Zentner J, Honegger J, Feuerstein TJ (2005) *Biochem Pharmacol* 69:169–178.
35. Pertwee RG (1997) *Pharmacol Ther* 74:129–180.
36. Ginovart N (2005) *Mol Imaging Biol* 7:45–52.
37. Lee CM, Farde L (2006) *Trends Pharmacol Sci* 27:310–316.
38. Kapur S, Zipursky RB, Remington G (1999) *Am J Psychiatry* 156:286–293.
39. Vogt BA, Laureys S (2005) *Prog Brain Res* 150:205–217.
40. De Jesus ML, Salles J, Meana JJ, Callado LF (2006) *Neuroscience* 140:635–643.
41. Gifford AN, Bruneus M, Gatley SJ, Lan R, Makriyannis A, Volkow ND (1999) *J Pharmacol Exp Ther* 288:478–483.
42. Hsieh C, Brown S, Derleth C, Mackie K (1999) *J Neurochem* 73:493–501.
43. Coutts AA, Anavi-Goffer S, Ross RA, MacEwan DJ, Mackie K, Pertwee RG, Irving AJ (2001) *J Neurosci* 21:2425–2433.
44. Kent RS, De Lean A, Lefkowitz RJ (1980) *Mol Pharmacol* 17:14–23.
45. Ross EM (1989) *Neuron* 3:141–152.
46. Barrero FJ, Ampuero I, Morales B, Vives F, de Dios Luna Del Castillo J, Hoenicka J, Garcia Yebenes J (2005) *Pharmacogenomics J* 5:135–141.
47. Patel S, Hamill T, Hostetler E, Burns HD, Gibson RE (2003) *Mol Imaging Biol* 5:65–71.
48. Patel S, Ndubizu O, Hamill T, Chaudhary A, Burns HD, Hargreaves R, Gibson RE (2005) *Mol Imaging Biol* 7:314–323.
49. Koeppe RA, Frey KA, Snyder SE, Meyer P, Kilbourn MR, Kuhl DE (1999) *J Cereb Blood Flow Metab* 19:1150–1163.
50. Yasuno F, Brown AK, Zoghbi SS, Krushinski JH, Chernet E, Tauscher J, Shaus JM, Phebus LA, Chesterfield AK, Felder CC, *et al.* (March 28, 2007) *Neuropsychopharmacology*, 10.1038/sj.npp.1301402.